31st International Conference
ENGINEERING MECHANICS 2025
Medlov, Czech Republic, May 12 –14, 2025
Paper **#41,** pp. 21–24, doi: 10.21495/em2025-21

PREDICTION OF UNIAXIAL AND BIAXIAL RATCHETING BY THE CHABOCHE MODEL WITH EVOLUTION FOR 304 STAINLESS STEEL

Adamec T.[1], **Kondepati S. K.**[2], **Petruška J.**[3], **Šebek F.**[4]

Abstract: *The precision requirements for cyclic plasticity models are often not very high in industrial applications, even though the integrity of many components subjected to cyclic plasticity is critical. Despite its limitations, such as poor prediction of ratcheting behaviour, the Chaboche model remains the most widely used model of cyclic plasticity. This paper presents the calibration of this model for uniaxial and multiaxial cyclic data on 304 stainless steel. The model incorporates a strain memory surface dependence to account for pronounced cyclic hardening. Resulting simulations carried out by calibrated model are used to highlight some of the modelling limitations.*

Keywords: Cyclic behaviour, Hardening, Low-cycle fatigue, Parameter evolution, Strain memory surface

1. Introduction

Cyclic plasticity, characterized by alternating plastic deformation, is a material behaviour observed in various engineering applications, including structural components in engines and piping systems. Its accurate modelling through numerical simulations is essential to predict material performance and ensure structural reliability. One of the most commonly used material models for cyclic plasticity is the Chaboche model, or Chaboche kinematic hardening rule, proposed by Chaboche et al. (1979), particularly because of its simplicity and availability in commercial software packages. One of the drawbacks of this model is its tendency to overpredict the ratcheting behaviour. This paper demonstrates that for certain materials, specifically 304 stainless steel, the Chaboche model can provide a reasonable prediction of ratcheting. Uniaxial and multiaxial ratchetings are studied. Therefore, the Chaboche model with modification proposed by Delobelle et al. (1995), which has no effect for uniaxial loading, is adopted. The complexity of the model is further increased by incorporating strain memory surface, initially introduced by Chaboche et al. (1979) and later refined through the addition of an evanescent term by Nouailhas et al. (1985).

2. Experiments

The experimental data for the 304 stainless steel used in this paper were taken from Hassan and Kyriakides (1994). These comprised 1 single-amplitude uniaxial strain-controlled test with a strain amplitude of 0.01, 6 uniaxial stress-controlled tests with varying stress amplitudes and mean stresses having mean stresses $\pm$ stress amplitudes of 19 $\pm$ 236 MPa, 36 $\pm$ 220 MPa, 36 $\pm$ 236 MPa, 36 $\pm$ 250 MPa, 36 $\pm$ 268 MPa and 47 $\pm$ 236 MPa and 3 biaxial strain-controlled tests with constant internal pressure, all with the same strain amplitude of 0.005 and different internal pressures resulting in circumferential stresses σ^{θ} of 28, 56 and 79 MPa.

[1] Ing. Tomáš Adamec: Brno University of Technology, Faculty of Mechanical Engineering, Institute of Solid Mechanics, Mechatronics and Biomechanics; Technická 2896/2; 616 69, Brno; CZ, Tomas.Adamec@vutbr.cz
[2] Sudhir Kumar Kondepati, M.Sc.: Brno University of Technology, Faculty of Mechanical Engineering, Institute of Solid Mechanics, Mechatronics and Biomechanics; Technická 2896/2; 616 69, Brno; CZ, Sudhir.Kumar.Kondepati@vutbr.cz
[3] prof. Ing. Jindřich Petruška, CSc.: Brno University of Technology, Faculty of Mechanical Engineering, Institute of Solid Mechanics, Mechatronics and Biomechanics; Technická 2896/2; 616 69, Brno; CZ, petruska@fme.vutbr.cz
[4] doc. Ing. František Šebek, Ph.D.: Brno University of Technology, Faculty of Mechanical Engineering, Institute of Solid Mechanics, Mechatronics and Biomechanics; Technická 2896/2; 616 69, Brno; CZ, sebek@fme.vutbr.cz

3. Constitutive modelling

The present constitutive modelling follows a small strain theory, additive law defining the increment of the strain tensor $\mathrm{d}\underline{\varepsilon}$, Hooke's law defining the increment of the elastic strain tensor $\mathrm{d}\underline{\varepsilon}^e$, associative flow rule defining the increment of the plastic strain tensor $\mathrm{d}\underline{\varepsilon}^p$ with the assumption of the von Mises yield function and combined hardening as

$$\mathrm{d}\underline{\varepsilon} = \mathrm{d}\underline{\varepsilon}^e + \mathrm{d}\underline{\varepsilon}^p = \frac{1+\nu}{E}\mathrm{d}\underline{\sigma} - \frac{\nu}{E}\mathrm{tr}\left(\mathrm{d}\underline{\sigma}\right)\underline{I} + \frac{3}{2}\frac{\underline{s}-\underline{a}}{\sigma^y + R}\mathrm{d}p, \tag{1}$$

where ν is the Poisson's ratio, E is the Young's modulus, $\mathrm{d}\underline{\sigma}$ is the increment of the stress tensor, $\mathrm{tr}()$ is the trace of the tensor, $\underline{I}$ is the unity tensor, $\underline{s}$ is the deviatoric stress tensor, $\underline{a}$ is the deviatoric backstress tensor, σ^y is the yield stress, R is the isotropic hardening and $\mathrm{d}p$ is the increment of the accumulated plastic strain. The von Mises yield function assumes the combined hardening as

$$f = \sqrt{\frac{3}{2}\left(\underline{s}-\underline{a}\right) : \left(\underline{s}-\underline{a}\right)} - \left(\sigma^y + R\right), \tag{2}$$

where : is the double dot product. The yield surface evolves according to the combination of Voce isotropic hardening defined as

$$\mathrm{d}R = b\left(Q - R\right)\mathrm{d}p, \tag{3}$$

where b and Q are the material parameters and Chaboche kinematic hardening with the modification by Delobelle et al. (1995) defined as

$$\mathrm{d}\underline{a} = \sum_{i=1}^{4}\left(\mathrm{d}\underline{a}_i\right) = \sum_{i=1}^{4}\left(\frac{2}{3}C_i\mathrm{d}\underline{\varepsilon}^p - \gamma_i\left(q\right)\left(\underline{a}_i\delta'\left(q\right) + \left[1-\delta'\left(q\right)\right]\left(\underline{a}_i : \underline{n}\right)\underline{n}\right)\mathrm{d}p\right), \tag{4}$$

where C_i, $\gamma_i\left(q\right)$ and $\delta'\left(q\right)$ are the material parameters, q is the radius of the strain memory surface and $\underline{n}$ is normal to the yield surface defined as

$$\underline{n} = \sqrt{\frac{3}{2}}\frac{\underline{s}-\underline{a}}{\sigma^y + R}. \tag{5}$$

The formulation of the strain memory surface that accounts for a possible reduction in the surface size governed by an evanescent term is defined as

$$g\left(\underline{\varepsilon}^p - \underline{Y}\right) = \sqrt{\frac{2}{2}\left(\underline{\varepsilon}^p - \underline{Y}\right) : \left(\underline{\varepsilon}^p - \underline{Y}\right)} - q, \tag{6}$$

$$\mathrm{d}q = \left(\eta H\left(g\right)\left\langle\underline{n} : \underline{n}^\star\right\rangle - \zeta\left[1 - H\left(g\right)\right]q^m\right)\mathrm{d}p, \tag{7}$$

$$\mathrm{d}\underline{Y} = \sqrt{\frac{3}{2}}\left(1-\eta\right)H\left(g\right)\left\langle\underline{n} : \underline{n}^\star\right\rangle\underline{n}^\star\mathrm{d}p, \tag{8}$$

$$\underline{n}^\star = \frac{\underline{\varepsilon}^p - \underline{Y}}{\sqrt{\left(\underline{\varepsilon}^p - \underline{Y}\right) : \left(\underline{\varepsilon}^p - \underline{Y}\right)}}, \tag{9}$$

where g is the strain memory surface function, $\underline{Y}$ is the centre of the strain memory surface, η, ζ and m are the material parameters, $<>$ are the Macaulay brackets, $H()$ is the Heaviside step function and $\underline{n}^\star$ is the normal to the strain memory surface. The strain memory surface dependence was introduced into the model through the evolution as

$$\mathrm{d}\gamma_i = D_{\gamma_i}\left(a_{\gamma_i} + b_{\gamma_i}\mathrm{e}^{-c_{\gamma_i}q} - \gamma_i\right)\mathrm{d}p, \tag{10}$$

$$\mathrm{d}\delta' = D_{\delta'}\left(a_{\delta'} + b_{\delta'}\mathrm{e}^{-c_{\delta'}q} - \delta'\right)\mathrm{d}p, \tag{11}$$

where a_{γ_i}, b_{γ_i}, c_{γ_i}, D_{γ_i}, $a_{\delta'}$, $b_{\delta'}$, $c_{\delta'}$ and $D_{\delta'}$ are the material parameters. Both γ_i and δ' start at certain initial values, which are also material parameters.

4. Calibration of the model and numerical simulations

The evolution of three backstresses with respect to the strain memory surface and Voce isotropic hardening were assumed, so the model has 33 material parameters in total. The calibration of the model was divided into two phases. First, an initial guess of the material parameters was made. Then, refinement of the material parameters was performed with an optimization algorithm that iteratively simulates experimental conditions with varying sets of material parameters and evaluates their accuracy. This process was carried out in two phases. In the first phase, all material parameters were optimized except for the elastic constants, which were estimated directly from experiments, and for the material parameters that control the evolution of δ'. The error function was designed to minimize the difference between numerical simulations and experimental for both uniaxial strain- and stress-controlled tests. The critical features to capture included the shape of the stabilized loop in the uniaxial strain-controlled test and the stabilized ratcheting rates in the stress-controlled tests, while secondary considerations encompassed the evolution of loop shapes in the strain-controlled test, the stabilized loop shapes in the stress-controlled tests and the monotonic responses. Given the large number of material parameters optimized in the first phase, a population-based method was used, namely, differential evolution. During the second phase, only 5 material parameters controlling the evolution of δ', which are relevant only in multiaxial loading, were optimized. The optimization algorithm was changed to Bayesian optimization using Gaussian process regression and probability of expected improvement and acquisition function due to the longer simulation time and the fewer material parameters being optimized. The calibrated model was used for the numerical simulations below. Left Fig. 1 shows a simulation of uniaxial strain-controlled test, where both the shape of the stabilized loop and the evolution of the loops were well simulated. However, the model was unable to fit the monotonic response.

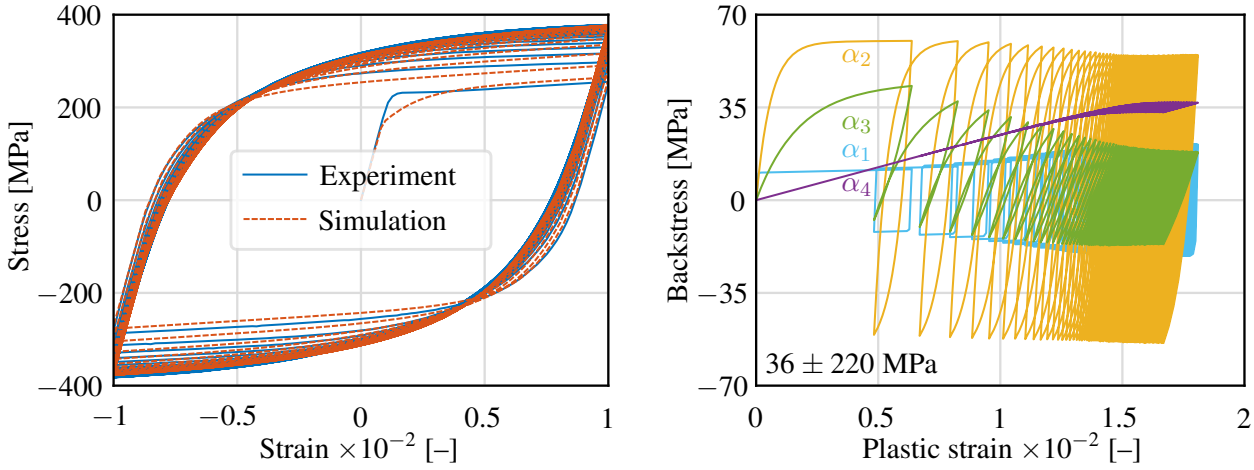

Fig. 1: Uniaxial strain-controlled (left) and stress-controlled (right) tests

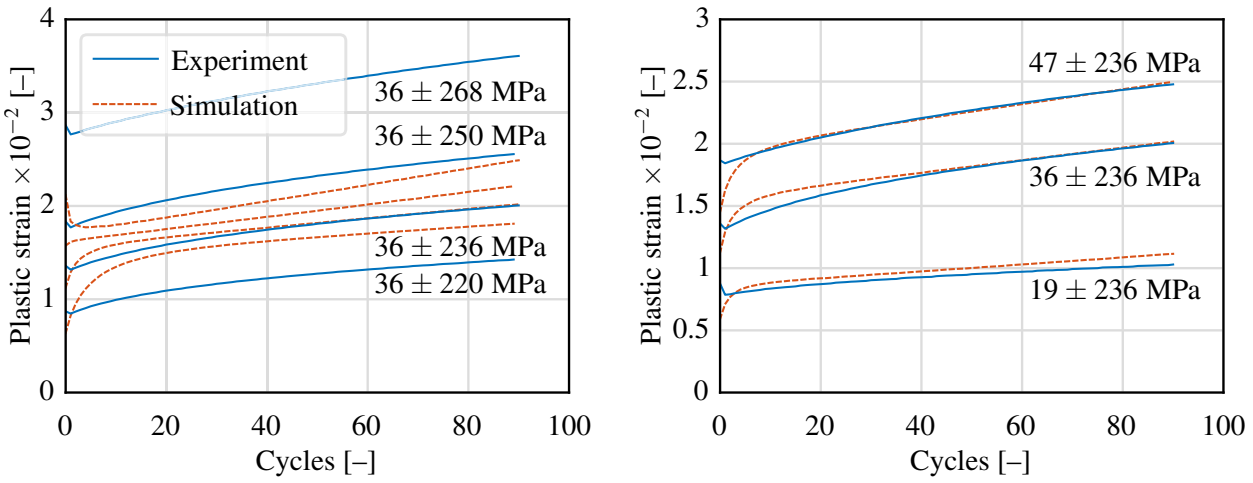

Fig. 2: Positive peaks of plastic strain for uniaxial stress-controlled tests

Fig. 2 shows that the model was able to fit the stabilized ratcheting rate for all experiments. The shape of the stabilized loops was also well simulated (left Fig. 3). However, the positive peaks of plastic strain of the experiments and simulations differed significantly for some experiments. This was caused by the simulated transient behaviour, a distinctive feature of the Chaboche model, caused by the decay of the ratcheting rate in the stabilization process of the mean values of individual backstresses. It is depicted in right Fig. 1, where the individual backstress components $\alpha_1, \ldots, \alpha_4$ are shown for the simulation of a uniaxial stress-controlled experiment. The differences were also due to the poor fit of the monotonic response, which is due to the use of a very small γ_4 to compensate for the tendency of the Chaboche model to overpredict the ratcheting rate. The monotonic response is often different from the cyclic one due to the loading prehistory. Furthermore, the precise fit of the monotonic response is often neglected to some extent because it can vary between specimens. Then, even small deviations in stress can cause quite large deviations in plastic strain for stress-controlled loading. Moreover, right Fig. 3 shows positive peaks of circumferential strain from biaxial ratcheting experiments with the stabilized ratcheting rates simulated quite well for all tests.

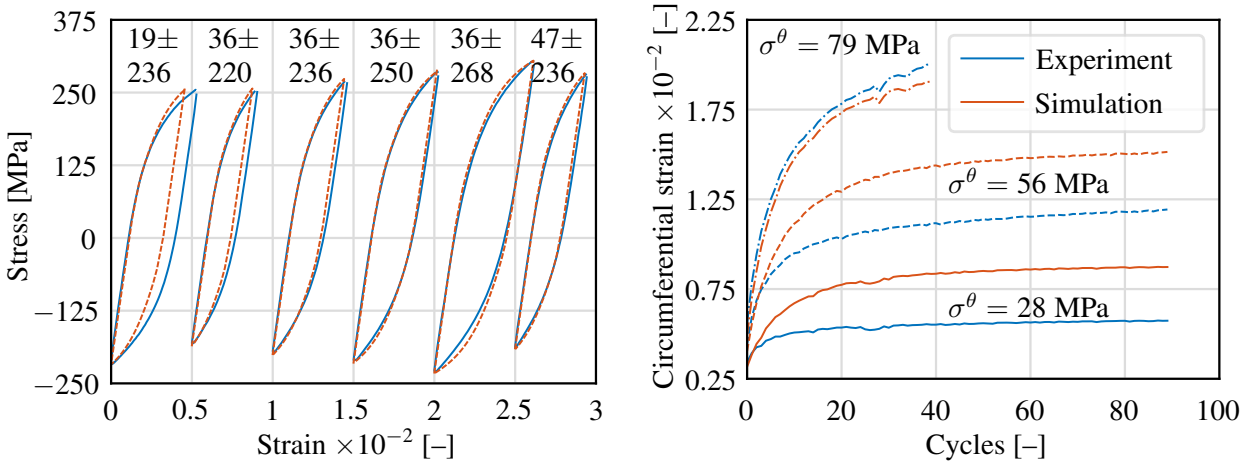

Fig. 3: Loops of stress-controlled (left) and positive peaks of circumferential strain of biaxial (right) tests

5. Conclusions

This paper showed that the modified Chaboche model is able to satisfactorily predict both uniaxial and multiaxial ratcheting rates in the case of 304 stainless steel. The main weakness of the prediction is the incorrect plastic strains. This reason was identified to be the transient behaviour of the model in case of uniaxial simulations and the inability to choose a correct value of the last material parameter of the kinematic hardening to fit the monotonic response due to fitting the stabilized uniaxial ratcheting rates.

Acknowledgements

This work is an output of the project Computational modelling of ductile fracture of identical wrought and printed metallic materials under ultra-low-cycle fatigue created with financial support from the Czech Science Foundation under the registration no. 23-04724S.

References

Delobelle, P., Robinet, P. and Bocher, L. (1995) Experimental study and phenomenological modelization of ratcheting under uniaxial and biaxial loading on an austenitic stainless steel. *International Journal of Plasticity*, 11, 4, pp. 295–330.

Hassan, T. and Kyriakides, S. (1994). Ratcheting of cyclically hardening and softening materials: I. Uniaxial behavior. *International Journal of Plasticity*, 10, 2, pp. 149–184.

Chaboche, J. L., Dang Van, K. and Cordier, G. (1979) Modelization of the strain memory effect on the cyclic hardening of 316 stainless steel. In *Proceedings of the Fifth International Conference on Structural Mechanics in Reactor Technology*, Berlin. International Association for Structural Mechanics in Reactor Technology, Raleigh, pp. 1–10.

Nouailhas, D., Cailletaud, G., Policella, H., Marquis, D., Dufailly, J., Lieurade, H. P., Ribes, A. and Bollinger, E. (1985) On the description of cyclic hardening and initial cold working. *Engineering Fracture Mechanics*, 21, 4, pp. 887–895.